

PAPER • OPEN ACCESS

## Shell effects and free-electrons in electromigrated oxidized Cu-nanocontacts


To cite this article: Julia Hauser *et al* 2023 *Nanotechnology* **34** 175703

View the [article online](#) for updates and enhancements.

You may also like

- [Structure and local charging of electromigrated Au nanocontacts](#)  
D Arnold, M Marz, S Schneider et al.
- [Quasiclassical theory of non-adiabatic tunneling in nanocontacts induced by phase-controlled ultrashort light pulses](#)  
Sangwon Kim, Tobias Schmude, Guido Burkard et al.
- [Formation of gold nanocontacts in an ultrahigh vacuum transmission electron microscope: A kinetic Monte Carlo simulation](#)  
S. V. Kolesnikov, I. N. Kolesnikova, A. L. Klavsyuk et al.

# Shell effects and free-electrons in electromigrated oxidized Cu-nanocontacts

Julia Hauser<sup>1</sup>, Daniel Rothhardt<sup>2</sup>, Robert Pfender-Siedle<sup>1</sup> and Regina Hoffmann-Vogel<sup>2</sup> 

<sup>1</sup>Physikalisches Institut, Karlsruhe Institute of Technology, D-76128 Karlsruhe, Germany

<sup>2</sup>Department of Physics and Astronomy, University of Potsdam, D-14476 Potsdam-Golm, Germany

E-mail: [regina.hoffmann-vogel@uni-potsdam.de](mailto:regina.hoffmann-vogel@uni-potsdam.de)

Received 9 September 2022, revised 20 January 2023

Accepted for publication 26 January 2023

Published 13 February 2023



CrossMark

## Abstract

Electromigration in interconnects continues to be an important field of study in integrated circuits as the interconnects are planned to shrink in size at comparable pace as the semiconductor functional elements. Through shrinking the interconnects approach the regime where quantum size effects become important. The observation of quantum size and shell effects is usually restricted either to low-temperatures or vacuum conditions or to chemically inert materials such as Au. Here, we show that in electromigrated Cu nanocontacts such effects can be observed at room temperature and room pressure even in the presence of oxidation. Our data provide evidence that the nanocontacts are nearly spherical objects with a triangular-cylindrical symmetry of their electronic wave functions with a stronger free-electron-like character compared to previous results. We do not observe a detrimental effect of oxygen. The presence of shell effects has implications for the technological use of Cu nanocontacts as interconnects in integrated circuits and could lead to the use of electronic wave functions of shells in such interconnects.

Supplementary material for this article is available [online](#)


Keywords: nanocontacts, electromigration, shell effects

(Some figures may appear in colour only in the online journal)

## 1. Introduction

In a small spatial area, confined electrons form discrete electronic states organized in electronic shells. This is well-known from the periodic table of elements, but also from semiconductor quantum dots, ‘artificial atoms’ [1]. For metals, these effects are more difficult to observe due to the larger electron density that causes a smaller Fermi-wavelength of comparable size to an atom. One way to observe these shell effects in metals is to study the abundance of metallic atomic-size clusters. Their abundance depends not only on their atomic, but also on their electronic configuration which is well-known to form shells.

Completed shells cause ‘magic’ numbers of cluster sizes that are more abundant than clusters with partly filled electronic cluster shells. Another way to observe them is to use electronic nanocontacts, as has first been done in the alkali metal Na [2, 3], where a large number of peaks in conductance histograms has been studied. The conductance of nanocontacts has been obtained from free-standing metallic bridges while the electrodes are pulled apart by bending the device in mechanically controlled break junctions. The conductance measured during mechanical deformation has been stored in a histogram to find out which conductances are more abundant. A simple estimate allows to link the nanocontact’s cross section  $A$  to the measured conductance  $G = \pi A$ , see [4]. The atomic structure of the metal allows to add only integer atoms, i.e. a given area to the cross-section of the nanocontact. Since a closed shell adds to the radius of the cross-section, structures periodic in the squareroot of the conductance are expected due to shell filling as has been

 Original content from this work may be used under the terms of the [Creative Commons Attribution 4.0 licence](#). Any further distribution of this work must maintain attribution to the author(s) and the title of the work, journal citation and DOI.

observed for Na, see [3]. Since a given amount of electrons is added to the nanocontact for each atom added, in the simplest view this applies to both, atomic and electronic shell effects.

For other materials such as work-hardened Au nanowires [5] also shell filling effects have been observed. Shell filling was identified by the position of prominent peaks in a conductance histogram with increasing distance between the peaks for increasing conductance [3]. Metallic nanocontacts are often investigated at low temperatures, where defects or less favorable atomic configurations are frozen in. This leads to an unspecific background of the conductance and causes smearing of sharp conductance peaks. In this way the resolution in the data is reduced. Scientific questions such as the one whether cylindrical shells or spherical shells are most relevant remain difficult to answer. Also oxygen has been suspected to cause an unspecific background and weaken conductance peaks in histograms obtained using the break-junction technique [6].

As a step forward, the conductance of metallic nanocontacts has been studied during and after electromigration where the nanocontacts are heated rather than cooled [7, 8]. In these works, the contacts were thinned in a controlled way using an electromigration algorithm [9]. Compared to low temperature studies, a larger number of sharp relevant peaks were observed in the same conductance interval with only limited broadening by thermal effects or by the change of the applied voltage. Different periodicities in the conductance have been observed and have been assigned to different crystallographic orientations of the nanocontacts [7, 10]. Both work-hardening and electromigration lead to enhanced local heating increasing the probability of the nanocontact to find structural equilibrium [10]. In this way the structural properties of the nanocontacts are enhanced compared to methods based on pulling at low temperature.

Here, we investigate shell effects in electromigrated naturally oxidized Cu nanocontacts. We show that Joule heating during a computer-controlled electromigration thinning process enhances shell effects in nanocontacts. We compare several ways of analyzing the data, and show that independently of the analysis, shell effects are clearly observed in the data. In addition, we show that the nearly spherical shape and triangular-cylindrical electronic structure of the shells reflects in the data. Also in the presence of oxygen sharp conductance peaks with a low unspecific background are observed for electromigrated nanocontacts. The annealing by heating has a more important sharpening effect on the conductance peaks compared to possible smoothing due to oxidation.

## 2. Experimental methods

To prepare Cu thin film wires we used Si substrates covered by a 500 to 1000 nm thick thermally oxidized layer for electrical insulation. Stainless steel masks with slit-shape openings were then placed in front of the substrate. The length of the slit in the mask was between 4 and 8 mm and its width between 30 and 500  $\mu\text{m}$ . We prepared Cu nanowires by sputtering between 27

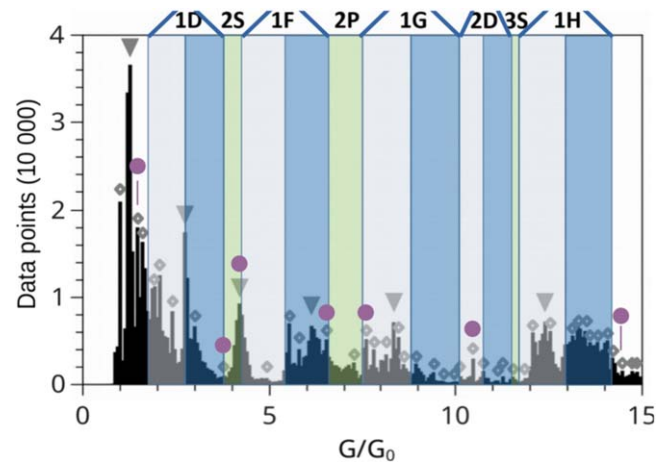


**Figure 1.** Histogram of oxidized electromigrated Cu nanocontacts obtained from electromigration thinning 40 samples. The six most prominent peaks have been marked by gray triangles. The magenta circles show the peaks derived from the magic numbers generally known in literature for Cu, as listed in column 1 of table 1. Additional peaks used for counting have been marked by gray open diamonds. 3d shells for spherical symmetry are marked above the graph. Starting from d shells, the first half of the shell is marked in blue, the second half of the shell is marked in green. S and p shells are marked in green. The bin size in this plot is 0.066  $G_0$ .

and 54 nm of Cu onto the substrate through the mask at a pressure of the vacuum chamber below  $10^{-3}$  Pa and a sputtering rate of 18 nm  $\text{min}^{-1}$ . Part of the samples were contacted using silver paste, others were contacted using Al bond wire.

Controlled electromigration was carried out in air and at room temperature. The process is designed to limit the maximally dissipated power in the junction during thinning while the resistance of the junction changes as a function of time [9]. Original conductance versus time traces have been shown in [10]. The electromigration algorithm increases the resistance in cycles [9]. During an electromigration cycle the voltage was increased in a stepwise manner until heating was detected as an absolute increase of the resistance. When a pre-chosen value of the resistance was reached the cycle was stopped and the next cycle was started at 60% of the last voltage in order to allow the contact to cool down. After that the resistance value for stopping the cycle was increased by a pre-chosen step [10].

To obtain conductance data during the full electromigration thinning process the current and imposed voltage were measured with a Keithley 2400 sourcemeter in a computer-controlled process. To obtain the conductance the current was divided through the voltage and the inverse of the starting conductance was subtracted from the inverse of the conductance. For more experimental details, see the supplementary material, section 1 and compare with [10, 11].

## 3. Results and discussion

We store the conductance values measured from 40 samples during heating in a histogram as a function of the conductance quantum  $G_0 = 2e^2/h$  (figure 1). During electromigration

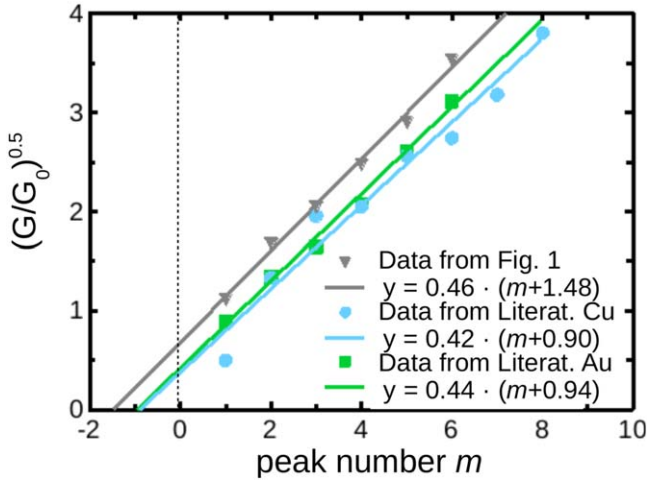


**Figure 2.** Gray triangles: squareroot of the conductance obtained from the six most prominent peaks taken from figure 1. Blue spheres: peaks expected for the magic numbers generally known for Cu clusters from literature as listed in column 1 of table 1. The squareroot of the conductance has been calculated as discussed in the main text and as listed in the fifth column of table 1. Green squares: peaks expected for the values known for Au work hardened nanocontacts from [5].

thinning, more stable atomic states lead to longer conductance plateaus and to stronger peaks in the conductance histogram. Due to different numbers of electromigration cycles for each sample, peak heights from different samples may differ. The histogram reflects the properties of an ensemble of oxidized Cu nanocontacts, oriented in different crystallographic directions that have a different atomic periodicity [10]. From the atomic periodicities it was found that the nanowires have a significant  $\text{Cu}_2\text{O}$  component [10] as was confirmed by cross-sectional scanning electron microscopy for larger wires [12].  $\text{Cu}_2\text{O}$  is detected because electrons with the Fermi wavelength of Cu travel through a structure of atomic periodicity known for  $\text{Cu}_2\text{O}$ .

We expect that most of the peaks show atomic periodicity rather than shell effects. For small peaks the question arises whether they are caused by fluctuations or by the physics of the system. Here, we consider all peaks that can be distinguished from neighboring peaks and that are observable even for variable bin size. The effect of variable bin sizes is shown in the supplementary material, section 2.

First, we take only the six most prominent peaks (gray triangles in figure 1). We then plot the squareroot of the conductance as a function of peak number  $m$ , figure 2 and we obtain a nearly straight line. Consecutive shells fill according to  $N^2$ , where  $N$  is the number of atoms. We conclude that the squareroot of the conductance of these peaks increases in regular steps, pointing to shell effects. Also for the data from [5], where Au was investigated, and for the magic numbers known from Cu clusters, nearly straight parallel lines are obtained. The origin of the peak number  $m$  obtained for Cu from our experimental data is shifted to the left by about 0.56 peak numbers. This suggests that another peak could be present at lower conductance values, see supplementary material, section 3. To evaluate peaks below  $1 G_0$  in more

detail we have additionally calculated the conductance difference of consecutive conductance measurements, see supplementary material, section 4. Indeed, additional peaks are observed below  $1 G_0$ . In summary, based on this first approach we conclude that the six most prominent peaks result from shell effects.

More precisely, we calculate the radius times the Fermi wavevector of the nanowire by using the semiclassical approximation from the conductance [2]

$$\frac{G}{G_0} \approx \left( \frac{k_F \cdot R}{2} \right)^2 - \frac{k_F \cdot R}{2}, \quad (1)$$

where  $k_F$  is the Fermi wavevector of the material and  $R$  is the radius of the cluster. The shape of the nanowire could depend on its formation process. In the past, the conductance of nanowires has mainly been investigated by mechanically controlled break junctions. In spite of the impact of different possible shapes of the nanowire, the number of atoms in a nanowire has been described suitable by formulae intended for clusters [13]. Here, we create nanowires by heating where often spherical objects are observed after the wire has been interrupted [14, 15]. For clusters of spherical symmetry

$$k_F \cdot R = 1.92 \cdot N^{(1/3)}, \quad (2)$$

see [2, 16, 17], where  $N$  is the number of atoms in the cluster.

In table 1 we compare the magic numbers expected for Cu clusters with the values we observe experimentally: 3d Cu magic clusters were found for  $N = 2, 8, 18, 20, 34$  and 40, see [18–20]. The peaks at 18 and 34 atomic numbers are specific for Cu, while additional peaks at 58 and 92 are known for alkali metals [2]. Oxidized Cu clusters have been considered in calculations, but the cluster sizes were limited [21].

The conductance values resulting from the magic numbers have been calculated (magenta spheres in figure 1 and column 3 in table 1). Indeed, we observe peaks near most of the magic number positions. The peak missing at  $0.25 G_0$  might be identified with one of the peaks observed below  $1 G_0$  and is discussed in more detail in the supplementary material, section 3. At  $3.81 G_0$  and at  $14.5 G_0$  small structures are observed. However, for most of the positions listed, the peaks are less prominent and only in one case, for  $4.18 G_0$ , the peak matches the most prominent peaks shown as gray triangles in figure 1. Since values from electromigrated Cu or temper hard Cu are not available, and most magic numbers are equal for Au and Cu, we compare to room temperature results using temper hard Au (column 4 in table 1) taken from [5]. For Au, peaks have been observed near 1.8, 4.3, 6.8, and  $9.7 G_0$  near the expected positions for 3d clusters.

While this explains the Au peaks well, it does not explain the experimentally observed conductance values of the most prominent peaks for Cu (gray triangles in figure 1, bold values in column 5 in table 1). We calculate the expected magic numbers (column 7 in table 1) from the experimentally observed peak positions (column 5). The experimentally observed most prominent peaks in Cu match better to peaks resulting from a cylindrical symmetry with triangular basis [22, 23] while the Au ones match the 3d spherical ones. For triangular disks [22, 23] the magic numbers 2, 6, 12, 20, 30

**Table 1.** Comparison of expected electronic shell effect peak positions with experimentally found ones. The two arrows start at the input values for calculations and end at the output values. Column 1–4 shows the expectations: the first column shows the expected magic numbers for free three-dimensional Cu clusters taken from [18]. The second column calculates the expected  $k_F \cdot R$  values from column 1 and the third column calculates  $G/G_0$  from column 2. Column 4 compares these expectations with the results for work hardened Au ([5]). Columns 5–7 show the experimental results of this work: column 5 shows the peaks observed here with the six most prominent peaks marked in bold, small peaks in regular characters and extremely small peaks in brackets. In column 6 we calculate  $k_F \cdot R$  for the six most prominent peaks. Column 7 gives the magic numbers calculated from column 6. These magic numbers are often located between two magic numbers of column 1.

1	2	3	4	5	6	7
	→				→	
$N$ Magic Reference [18]	$k_F \cdot R$ Equation (2)	$G/G_0$ Equation (1)	$G/G_0$ Au [5]	$G/G_0$ Figure 1	$k_F \cdot R$ Equation (1)	$N$ Magic Equation (2)
2	2.42	0.25		—		
8	3.84	1.77	1.8	<b>1.25</b> 1.5	3.4	6
18	5.03	3.81	2.7	<b>2.8</b> (3.75)	4.5	13
20	5.21	4.18	4.3	<b>4.2</b>	5.2	20
34	6.22	6.56	6.8	<b>6.1</b> 6.6	6.0	31
40	6.57	7.50		7.6	6.6	41
58	7.43	10.09	~9.7	<b>8.4</b> 10.5	6.9	46
92	8.67	14.45		<b>12.4</b> (14.5)	8.1	75

and 42 are known and 46 is known for a cylindrical shape. These often match or nearly match the average value of two expected magic numbers, i.e.  $6 \approx 5 = 1/2(2 + 8)$ ,  $13 = 1/2(8 + 18)$ ,  $31 \approx 30 = 1/2(20 + 40)$ ,  $46 \approx 49 = 1/2(40 + 58)$  and  $75 = 1/2(58 + 92)$ . For larger clusters, deviations occur as the next magic numbers are 56 (triangle) and 68 (cylinder). Considerations concerning the experimental precision of the peaks listed in table 1) are given in the supplementary material, section 5.

A simple shift in  $k_F R$ , as might be the result of a reduced number of electrons due to the CuO surrounding the nanocontacts, cannot explain the difference between expected magic numbers and observed most prominent peaks. Such a shift would affect all of the values, but here, the calculated peaks observed for 20-atom and possibly the 40-atom cluster match the experimental observation. However, a registry between the expected magic numbers and the observed ones is observed, as expected for the relation between 2d-triangular symmetry and 3d symmetry.

We have indicated in figure 1 the shells for 3d spherical symmetry taken from [24, 25]. The most prominent peaks marked in gray triangles are mostly located at filled half-shells only one is located at a half-filled half-shell. Apart from the most prominent peaks also the conductance regions that form a particular shell show a structure: for the 1d and 1g shell, the

less than half-filled shell shows additional weight accompanied by additional fluctuations compared to the more than half-filled 1d and 1g shell, and for the 1f shell and the 1h shell, the more than half-filled shell shows an enhanced weight in the histogram. This structure is accompanied with more fluctuations for the 1f shell, but rather with less fluctuations for the 1h shell. No matter how the structure is described in detail, we conclude that shell effects do influence the histogram and that less than half-filled shells show a difference to more than half-filled shells in particular for the magnetic shells, i.e. d shells and higher.

Although we combine a three-dimensional view of the spherical shape of the nanowires with a two-dimensional view of electronic conduction through a nanowire (i.e. the nanowire cross-section is two-dimensional), the shell structure obtained describes the data correctly with the exception of the most prominent peaks that do not appear at the expected positions. For nanowires with a random range of prolonged or flattened shapes, we would expect a broadening of the shell structure. Here, in contrast we can clearly relate the shells to the experimental data. To test how precisely a peak can be assigned to a number of atoms, we use the width of the peak observed at  $G = 4.2 G_0$  to investigate the uncertainty in  $N$  that is caused by the width of the peak. The result is  $\Delta N = 1.1$ , a small number compared to most magic numbers. We



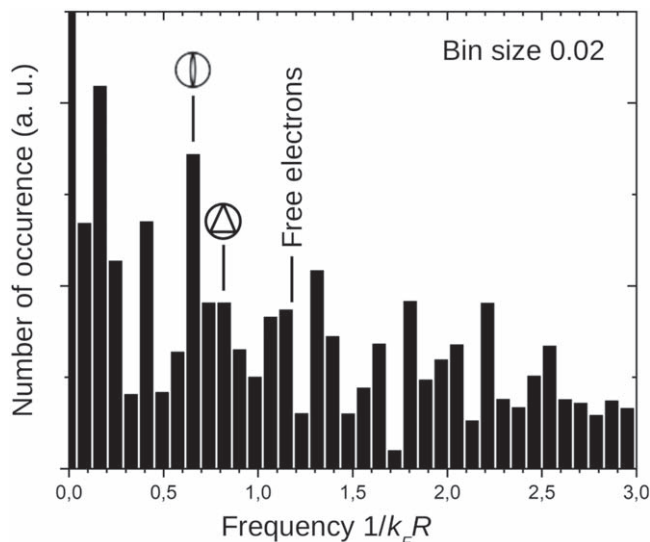


**Figure 3.** Fourier transform of the conductance histogram taken as a function of  $k_F R$ .  $k_F R$  has been calculated using equation (1) for the data shown in figure 1. Since the data range is reduced by calculating  $k_F R$ , the bin size has been reduced to 0.02.

conclude that the shape of the nanowires must be typically the same for all conductance values, pointing to a neither prolonged nor flattened but rather compact, nearly spherical shape.

Figure 3 shows the Fourier transform of the histogram taken as a function of  $k_F R$ . Different frequencies have first been predicted for different symmetry of the orbitals [26] and some of these frequencies have been observed experimentally in Cu nanocontacts pulled apart by the mechanically controlled break junction technique [13]. For the diametral and triangular orbits, frequencies of  $0.68/k_F R$  and  $0.83/k_F R$  are expected respectively. Here, we observe a peak near the expected position of the diametral orbit. At the expected position of the triangular orbit we observe a shoulder. In previous results, only the diametral orbit has been observed as a small peak, the triangular one was absent [13].

An additional peak is observed near  $1.1/k_F R$ . A related peak has been observed before in [13] at  $0.99/k_F R$ . From theory a small peak is expected at  $0.90/k_F R$  for the square orbit [26]. In the past, the peak at  $0.99/k_F R$  has been attributed to electrons that are better described as free electrons compared to the treatment in [26]. A shift has been predicted for more free-like electrons, and especially for a softer potential rise at the surface of the nanowire [23]. A value up to  $1.2/k_F R$  is expected [23], while the diametral and triangular peaks remain unchanged. The value of  $1.1/k_F R$  we observe here fits well into this picture. Additional peaks from higher order orbits (square, hexagonal,...) are expected at higher  $1/k_F R$  values. The main difference to previous results is that the weight of the free electron-like peak was larger in previous results than the weight of the diametral peak, in contrast to predictions. Here, the diametral peak is more important than the peak assigned to free electrons and the shift towards more free electron-like behavior is larger.

The weight of the frequencies gives us information about the symmetry of the electronic wave functions. We conclude that the wave functions are rather free-electron like and have a clearly cylindrical symmetry with possible triangular influences and that the shape deduced from the atomic number of the nanowire is compact, possibly spherical. Due to shell filling rules, we expect that half-filled shells and half-filled half-shells are points of maximal magnetic moments [27]. These are the energetically most favourable points in our oxidized Cu nanocontacts in contrast to Au nanocontacts and could indicate an enhancement of magnetically influenced electronic states. This should be investigated further by studies including a magnetic field.

#### 4. Conclusion

In summary, electronic shell effects are observed in electro-migrated Cu nanocontacts even at room temperature and in the presence of oxydation. Several possibilities for the assignment of shells are discussed. These reflect the cylindrical symmetry of the electronic wave functions while at the same time we show evidence for a nearly spherical shape of the nanocontacts. The nanocontacts show clear evidence for nearly free electrons that make them attractive as contact material for small transistor-like objects such as molecules. We do not observe evidence for the introduction of random structural defects due to oxydation.

#### Acknowledgments

We thank Marz and Sürgers for help with the experimental work. Financial support from the European Research Council through the Starting Grant NANOCONTACTS (No. 239 838), from the Ministry of Science, Research and Arts, Baden-Württemberg, in the framework of its Brigitte-Schlieben-Lange program and from a Heisenberg fellowship of the DFG is gratefully acknowledged.

#### Data availability statement

The data that support the findings of this study are available upon reasonable request from the authors.

#### ORCID iDs

Regina Hoffmann-Vogel  <https://orcid.org/0000-0003-4984-6210>

#### References

- [1] Chakraborty T 1999 *Quantum Dots: A Survey of the Properties of Artificial Atoms* (Amsterdam: North-Holland)

- [2] Yanson A I, Yanson I K and van Ruitenbeek J M 1999 *Nature* **400** 144
- [3] Yanson A I, Yanson I K and van Ruitenbeek J M 2001 *Phys. Rev. Lett.* **87** 216805
- [4] Agraüt N, Levy Yeyati A and van Ruitenbeek J M 2003 *Phys. Rep.* **377** 81
- [5] Yanson I K, Shklyarevskii O I, Csonka S z, van Kempen H, Speller S, Yanson A I and van Ruitenbeek J M 2005 *Phys. Rev. Lett.* **95** 256806
- [6] Thijssen W H A, Strange M, de Brugh J M J and van Ruitenbeek J M 2008 *New J. Phys.* **10** 033005
- [7] Hoffmann R, Weissenberger D, Hawecker J and Stöffler D 2008 *Appl. Phys. Lett.* **93** 043118
- [8] Hoffmann-Vogel R 2017 *Appl. Phys. Rev.* **4** 031302
- [9] Strachan D R, Smith D E, Johnston D E, Park T-H, Therien M J, Bonnell D A and Johnson A T C 2005 *Appl. Phys. Lett.* **86** 043109
- [10] Pfender-Siedle R, Hauser J and Hoffmann-Vogel R 2017 *Phys. Rev. B* **95** 235418
- [11] Stöffler D, Marz M, Kießig B, Tomanic T, Schäfer R, v Löhneysen H and Hoffmann-Vogel R 2014 *Phys. Rev. B* **90** 115406
- [12] Hauser J S et al 2016 *Appl. Phys. A* **122** 1068
- [13] Mares A I and van Ruitenbeek J M 2005 *Phys. Rev. B* **72** 205402
- [14] Stöffler D, Fostner S, Grütter P and Hoffmann-Vogel R 2012 *Phys. Rev. B* **85** 033404
- [15] Arnold D, Marz M, Schneider S and Hoffmann-Vogel R 2017 *Nanotechnology* **28** 055206
- [16] de Heer W A 1993 *Rev. Mod. Phys.* **65** 611
- [17] Brack M 1993 *Rev. Mod. Phys.* **65** 677
- [18] Kabir M, Mookerjee A and Bhattacharya A K 2004 *Phys. Rev. A* **69** 043203
- [19] Höppler C and Zwerger W 1998 *Phys. Rev. B* **59** R7849
- [20] Stepanyuk V S, Bruno P, Klavsyuk A L, Baranov A N, Hergert W, Saletsky A M and Mertig I 2004 *Phys. Rev. B* **69** 033302
- [21] Jdraque M and Martín M 2008 *Chem. Phys. Lett.* **456** 51
- [22] Reimann S M, Koskinen M, Helgesson J, Lindelof P E and Manninen M 1998 *Phys. Rev. B* **58** 8111
- [23] Reimann S M, Koskinen M, Häkkinen H, Lindelof P E and Manninen M 1997 *Phys. Rev. B* **56** 147
- [24] Knight W D, Clemenger K, de Heer W A, Saunders W A, Chou M Y and Cohen M L 1984 *Phys. Rev. Lett.* **52** 2141
- [25] Reber A C and Khanna S N 2017 *Acc. Chem. Res.* **50** 255
- [26] Ogando E, Zabala N and Puska M J 2002 *Nanotechnology* **13** 363
- [27] Reimann S M and Manninen M 2002 *Rev. Mod. Phys.* **74** 1283